Two-Port Network Models for Compliant Rhomboidal Strain Amplifiers

Joshua Schultz, Jun Ueda, *Member, IEEE*

***Abstract*—Piezoelectric stack actuators have the advantages of zero backlash and no acoustic noise, but their stroke is too small to actuate robotic links directly. Because the force available is often more than is required, the stroke of the piezoelectric stack can be amplified by a compliant mechanism at the expense of force. It is not always clear what the geometry of this compliant mechanism should be. Compliant mechanisms have parallels in biology in that they describe two-way interactions between the actuator and the environment. In this article, we employ the concept of a two-port network model from circuit theory to describe this two-way interaction, and present a method to obtain each element of the two-port model as an analytical function of physical geometric parameters for a wide class of geometries. This method makes use of Castigliano's theorem and Euler-Bernoulli linearly elastic beam theory. To our knowledge, this is the first two-port representation of a compliant mechanism that is based on analytical expressions of geometric parameters. This analytical model agrees well with finite element method calculations. We also examine a representative case experimentally and achieve accuracies better than 18%.**

I. Introduction

Although humanoid robots possess a human-like morphology, most do not possess human-like actuation. Traditional actuators used in most humanoids lack the two-way compliant interaction characteristic of biological motion systems, which is necessary to ensure safety when robots and humans share the same workspace. Biological muscle, rather than operating by relative rotation of rigid members, operates by contracting numerous flexible units in concert. This gives muscle several advantages with regard to interaction with an uncertain environment. Muscles also posses damage tolerance and can be synergistically activated to achieve desirable impedance characteristics [1].

Lead Zirconate Titante (PZT) stack actuators, although inorganic, are like biological muscle in that they exhibit a two-way interaction with the load. Piezoelectric stacks by themselves are of little use in robotics applications due to their minuscule displacement. To mitigate this, the piezoelectric stack actuator imposes a force-displacement boundary condition at a strategically chosen point (the input) on a linearly elastic deformable body. The geometric properties of the deformable body are such that the displacement at another particular point (the output) is much larger than the displacement of the input. The output point is connected to the load. Of course, some of the electrical energy supplied to piezoelectric stack is stored in the deformable body as strain energy, and in some sense this can be viewed as a parasitic effect.

Joshua Schultz and Jun Ueda are with the George W. Woodruff School of Mechanical Engineering, Georgia Institute of Technology, Atlanta, GA, 30332 USA e-mail: joshua.schultz@gatech.edu.

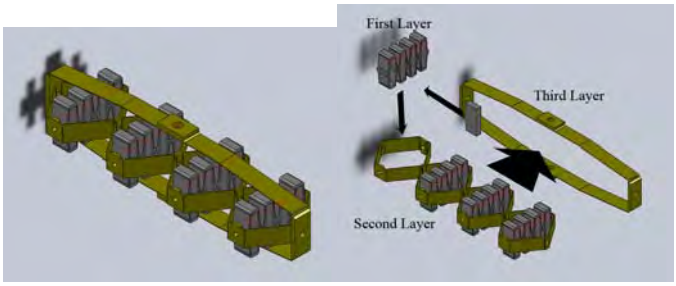

(a) hierarchical nested structure (b) exploded view

Fig. 1. Multilayer nested rhomboid compliant actuator

A summary of various techniques for optimizing these PZT plus compliant mechanism devices can be found in [2]. Design of a compliant mechanism has two distinct steps, a topology synthesis, followed by a dimensional synthesis [3]. One method is the "topological optimization" approach, whereby the designer begins with a "ground structure" [4], [5], usually a uniform truss with uniform members. The algorithm modifies, and in some cases removes these members, resulting in a topology. The thickness of various elements is refined during the dimensional synthesis phase, which does not change the path from active element to load. Grossard, et al. [6] use a variation on this approach using a component library of active and passive ground structures, called FlexIn. Their optimization routine also includes dynamic performance criteria. Although this "automatic" approach is appealing, it is computationally intensive, and the process does not apply engineering intuition in the intermediate stages of the process.

This research is concerned with a particular canonical topology, the rhomboid. This geometry lends itself well to large-displacement nested mechanisms, where the output of one compliant mechanism is the input to the next, such as in the mechanism shown in Fig. 1. This is necessary because for large-displacement actuators, manufacturing and space considerations do not allow the force-displacement tradeoff to be completed in a single stage. The rhomboidal strain amplification principle is illustrated in Fig. 2. If the major diagonal of a rhombus undergoes a change in length, the minor diagonal will undergo a much larger change in length, hence, a "strain amplification." The mechanism in Fig. 2 shows rigid links connected by hinges. This idealized mechanism is seldom used in practice. In general, rhomboids are small devices, and must be manufactured in one piece, precluding the use of actual hinges. Hinges pose assembly difficulties, can introduce backlash, and are subject to lubrication and contamination issues. So typically, mechanisms have "flexure

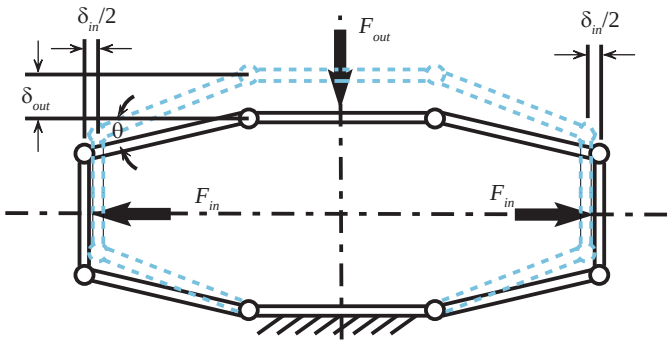

Fig. 2. rigid rhomboidal strain amplifier

hinges," points where additional material is removed to create a section with high localized compliance. The remainder of the structure is usually considered to be rigid. Of course, the hinges still possess some finite stiffness, so the displacement will always be less than that of the idealized mechanism. Most of the research on rhomboidal strain amplification methods focus on the design of these hinges and how closely they approximate ideal hinges [7]–[12].

In contrast with existing works, this research does not seek to merely add a set of expressions for yet another compliant mechanism geometry. It seeks rather to provide a critical ingredient for *the study of large displacement nested mechanisms*, by providing a concise model of a single rhomboid's behavior within a nested hierarchy. It presents a method to obtain simple input-output models of an entire class of compliant mechanisms with numerous choices of geometric parameterizations, not merely for flexure hinges. One important distinction to note is that the works referred to here are strictly for planar mechanisms, whereas the modularity and generality of the units described here allow them to be combined in 3 dimensional configurations. The method is demonstrated for one particular parameterization. Results are confirmed by numerical procedures and finite element methods. The idealized mechanism naturally give rise to the idea of "flexure hinges," perhaps explaining the direction of prior work, but there is no reason that compliance has to be localized. The methods presented in this paper work equally well for rhomboids with distributed compliance.

So-called "strain-amplified" piezoelectric stack actuators are currently available from a small number of vendors, however, even with an impressive displacement amplification factor of 10-20, [13], [14], the displacement is still on the order of μm, still not large enough for most robotics applications. Ueda, Secord, and Asada [15] amplify this displacement still further by placing several amplified stacks in series and amplifying the output of this series combination a second time, calling the strain amplifier of the commercial part the "first layer," and the rhomboidal mechanism that amplifies the output of the series combination the "second layer." This multi-stage amplification technique produces strains on the order of that of human muscle, approximately 22%. Since this actuator has a strain rate similar to that of human muscle, its displacement and force will scale with volume similarly to human muscle. For this reason, it is termed the *cellular actuator*, because many of them can be connected in series and parallel combinations to achieve desired actuation characteristics, as human muscle cells are. Secord and Asada [16], [17] combine this mechanism with mechanical stops so that the resulting actuator will have a position-dependent stiffness as specific units in the chain are activated.

This work presents an input-output understanding of each rhomboidal compliant mechanism in the hierarchy based on elementary mechanics of materials and two-port electrical network theory. This particular formulation is constructed so as to concisely but adequately describe interconnections of these mechanisms to construct a large-displacement actuator.

II. Two-port models of strain amplifying compliant mechanisms

According to Choma, [18], the two-port network is a simple way to model an electrical network when the mathematical models of the underlying components are either unknown, or inordinately cumbersome. The two-port concept allows the designer to analyze the network as a "black box" and focus on its input-output behavior, ignoring the constitutive relationships interior to the network. Input-output behavior can be described by simple passive impedances plus voltage-controlled current sources or current-controlled voltage sources interior to the network. Interested readers can find additional details in Appendix A.

With the appropriate mechanical-electrical analogies, two-port networks can also be used to model rigid body or flexextensional mechanical systems. This makes two-port networks a simple but powerful analysis tool, one that is particularly useful for describing the two-way interactions characteristic of biologically inspired actuation. Abdalla [4] et al. model not only the compliant mechanism as a two port network, but also the piezoelectric stack actuator itself. The four quantities of interest are the voltage applied to the stack, the charge stored in the stack, the force applied by the stack, and the stack displacement. Therefore, the electromechanical transduction of the PZT ceramic also lends itself to a two-port network description. For this reason, it is even more advantageous to model the compliant mechanism as a two-port network, for then the interconnection laws for two-port networks can simply and elegantly describe an entire multi-stage compliant device, and if the source impedance (electrical) and terminal impedance (mechanical) are known, the entire response can be predicted. If the immittance matrix is known for each compliant strain amplifying mechanism in a hierarchical nested configuration, the stiffness of the entire mechanism can be easily predicted, and can be accurately approximated even if only the outermost few layers are known [19]. Abdalla, et al. show some key properties of the two-port model approach, but do not explain how to determine the immittance matrix from the geometry and material properties of the compliant mechanism constituting each layer, necessitating the contribution described in this work.

The approach in [4] assumes that the designer begins the design with knowledge of the load impedance. They show that the compliant mechanism and the PZT stack can be designed

separately, in that order. They also derive an expression for the efficiency and show that it varies inversely with the geometric advantage (or displacement amplification factor) of the mechanism,

$$a = \frac{\delta_{out}}{\delta_{in}}. \quad (1)$$

They then begin with an assumed truss ground structure and numerically follow a topological optimization approach. The most efficient structure is the ground structure, which is the most rigid. They therefore use a quadratic cost function with weights on the geometric advantage and efficiency to arrive at an optimal compliant mechanism for the assumed load. While Abdalla's work highlights the benefits of two-port modeling for compliant mechanisms, it is not clear how well the mechanism will work across varying loads typical in robotics and how the model will vary with manufacturing tolerances, because it does not draw the connection between geometry and mechanism function in general.

Rhomboidal mechanisms are an intuitive topology and lend themselves well to interconnections in series, parallel, and nested configurations and can therefore be used to construct muscle-like robotic actuators. Another good rationale for using rhomboidal mechanisms is that automatically generated topology optimizations have converged to structures that are rhomboidal in shape [20]. Trying to achieve a desired stroke length with series combinations of piezoelectric stacks amplified a single time (such as the commercially available devices discussed later in the paper) results in an overall actuator that is too long relative to its stroke length.

III. Nested amplification mechanisms

To design a nested actuator, we begin with commercially available single-layer amplified PZT stacks, concatenate a small number of these in series, and amplify their displacement multiple times using compliant rhomboidal mechanisms. Each layer of amplification can be expressed as a two-port network. Ueda, Secord, and Asada [15] propose such a multi-layer strain amplified mechanism, using the concept of a two-port network. Rather than supplying connections to the mechanism's geometry, their immittance matrix parameters are related to the stiffnesses in a lumped parameter Hill muscle model. Using finite element methods, they develop a prototype two-layer actuator optimized for maximum output displacement given reasonable manufacturing constraints. However, this actuator has very low force capability and the design procedure was performed using ad hoc methods. It is not clear from this work how force-displacement specifications can be satisfied by a set of immittance parameters and how to determine the geometrical characteristics of the various layers that meet these performance specifications.

In essence, Ueda, Secord, and Asada [15] solve the "forward" problem: given a geometry, determine its performance characteristics. We would like to solve the "reverse" problem: given a set of performance specifications, determine the geometry characteristics that will meet these specifications, i.e., determine what compliant mechanisms allow a robot to supply required forces within the desired range of poses when a voltage is applied to a PZT stack. *It is the reverse problem that really benefits from an analytical model*. The two-port model of rhomboidal strain amplifying mechanisms presented in this article is a key step towards making the reverse problem easier to solve, because it encapsulates complicated geometric relationships in 3 elements per layer that are key to its input-output behavior. Optimization routines need to solve the forward problem multiple times in order to find an optimal point. To analyze complicated series-nested compliant actuators with multiple stages of amplification using finite element methods, great care needs to be taken with the mesh at interfaces, thin sections, and changes in cross section to ensure that the problem will be numerically solvable. Even if a search direction can be computed using finite differences, to perform a finite element simulation, a new CAD model needs to be constructed at each iteration. In addition, the finite element results give no insight on how to choose the trial geometry to get closer to the goal. This makes solving the reverse problem using finite element models extremely labor intensive. Our approach allows the designer to find an analytical model for a given choice of geometric parameterizations, and quickly get a sense of how changing each parameter affects the performance of the compliant strain amplifier and the nested mechanism as a whole. The forward problem is then merely a function evaluation, so common optimization routines can be used, provided the parameterization and constraints result in a convex problem. Search directions can be automatically computed from the analytical model, and the only CAD model that need be created is the one used for manufacture. Using the two-port formalism, it is easy to see how manufacturing tolerances will affect the performance of the entire device. The two-port model also shows clearly how each layer in a nested hierarchy contributes to the function as a whole.

IV. Finding expressions for the immittance parameters using Castigliano's theorem

Since we are planning to model a rhomboidal strain amplification mechanism as two-port network, we are less concerned with the internal stress and strain fields than the input-output behavior of the mechanism. For this reason, it is natural to use Castigliano's theorem [21], since it provides an input-output relationship between the loads on a structure and a displacement at a given point.

Castigliano's theorem has been used in several previous works to determine the stiffness of flexure hinges [8], [12]. Lobontiu and Garcia [9] characterize an entire hinged mechanism in terms of three parameters, the input stiffness, the output stiffness, and the displacement amplification and optimize the filleted flexure hinges to achieve a balance between amplification and stiffness, however, unlike a two-port model, it does not describe the function of the mechanism across varying loads and control inputs and was not formulated with large-stroke robotic applications in mind. In an actual compliant displacement amplification mechanism, the amplification factor will vary with loading conditions and along the stroke necessitating a slightly more involved description.

The bilateral two-port approach adds a level of abstraction that makes the problem tractable with larger numbers of parameters and is naturally suited to representing the two-way interactions of nested multi-stage compliant mechanisms.

Our analysis begins along the lines of the "chain method" described by Howell [22] for a simply connected body. Unlike Howell, we are not interested in a numerical evaluation of nodal displacements. Instead, we resolve the boundary conditions for a multiply connected body analytically, resulting in an analytical input-output model. In order to determine the two-port model of a general rhomboidal compliant mechanism, we make several simplifying, but justified, assumptions. First, we assume that the mechanism is symmetric about the two axes shown in Fig. 2. This allows us to derive the input-output relationships by analyzing a quarter mechanism. Second, we assume that forces are applied to a given layer only at the input and the output. Third, we assume that the compliant mechanism is composed of finitely many thin straight segments rigidly connected in series and fillet radii are small relative to the segment length and have negligible effect.

The method to determine the expressions for the immittances is summarized as follows: first, we resolve the static indeterminacy in the doubly connected rhomboid, eliminating the moment reaction in favor of the input and output forces. The internal moment reaction is a hidden parameter and is subsumed in the two-port formalism. This is possible because of the symmetry of the compliant mechanism. Second, we apply Castiglianos theorem in both the input and output directions. Third, we collect terms so that these two relations correspond to the two-port model relationships.

Consider a general single straight segment (i) rigidly connected to the preceding segment ($i-1$). The free body diagram is shown in Fig. 3. In this way, we can express the internal forces in a given segment in terms of its geometric parameters and the forces in the preceding segment. N_i is the internal axial load, V_i is the internal shear, M_i is the internal moment for segment i. z_i is the distance to a point on the segment, ranging from 0 to z_i^f. $\alpha(z)$ is the angular deflection at z_i. θ_i is the orientation of the segment in the undeformed configuration. Beginning with the reactions at a fixed flange (section 0), we can propagate the internal forces and moment outward through the quarter mechanism until we reach the point of application of the input force.

Applying the equations of static equilibrium to section i in matrix-vector form we can express the internal forces and moment in segment i at a distance along the segment z_i in terms of those in the preceding segment as:

$$\begin{bmatrix} N_i \\ V_i \\ M_i \end{bmatrix} = {}^{i}P_{i-1} \begin{bmatrix} N_{i-1} \\ V_{i-1} \\ M_{i-1} \end{bmatrix} \tag{2}$$

where

$${}^{i}P_{i-1} = \begin{bmatrix} \cos(\theta_i - \theta_{i-1}) & -\sin(\theta_i - \theta_{i-1}) & 0 \\ \sin(\theta_i - \theta_{i-1}) & \cos(\theta_i - \theta_{i-1}) & 0 \\ z_i \sin(\theta_i - \theta_{i-1}) & z_i \cos(\theta_i - \theta_{i-1}) & 1 \end{bmatrix}. \tag{3}$$

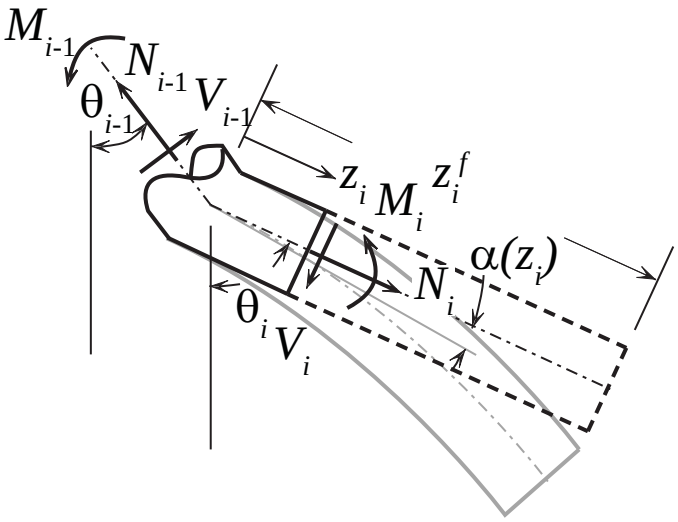

Fig. 3. Free body diagram of a general flexible segment with no loads applied to its interior.

To propagate this to the next segment, we evaluate (2) at $z_i = z_i^f$, which is a geometric parameter. The rhomboidal amplification layer is a doubly connected, statically indeterminate structure. In order to solve a doubly connected structure, we need additional compatibility conditions expressed in terms of the displacement, which we develop here. A generalized compliant mechanism that conforms to the assumptions above is shown in Fig. 4. $N_k, M_k, k = \{P, Q, R\}$ are the equivalent moment and axial reactions from the removed section. The circled numbers $\{1 \cdots N\}$ denote the index of each segment. R_x, R_y, and M_R are the reactions at the fixed end condition. To resolve the static indeterminacy, we proceed as follows: imagine that we cut the structure in half along A–A, discarding the right hand (light gray) half. A fixed end condition is then applied at point R. Due to symmetry about A–A, each half of the structure will carry half of the applied load F_{out}, and deform by the same amount in the direction of F_{out}. Therefore, the right half will impose no shear reaction on the left half. However, there will be a normal reaction force, N_P, imposed by the right half on the left half to insure that point P remains on the center line. The right half will also apply a moment reaction M_P on the left half, ensuring that the deflection angle of the final segment is continuous at P. These two compatibility conditions allow us to determine these unknown internal reactions.

Because the structure is also symmetric about B–B, the upper and lower quarters will each carry 1/2 of the load F_{in}, and deform by the same amount. This allows us to express the compatibility conditions at point Q, simplifying the results, and discard the upper, dark gray quarter, replacing by its internal reactions N_Q and M_Q. Because of symmetry about B–B, the internal reaction $N_Q = F_{out}/2$. Due to symmetry, the compatibility condition on the deflection angle stipulates that the tangent at Q must remain unchanged from its undeformed configuration, or:

$$\alpha(z_i^f) = \theta_N. \tag{4}$$

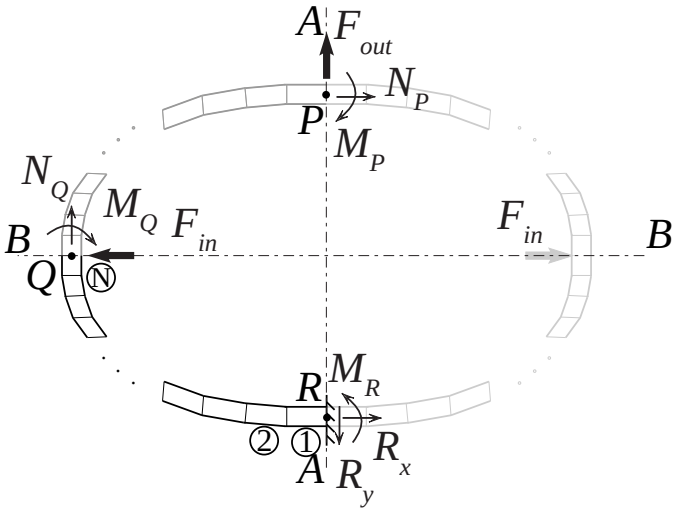

Fig. 4. Doubly symmetric actuator composed of straight segments

where α is the function for the deflection angle of segment i. In [9], [21], expressions for redundant reactions are found using Castigliano's theorem, but in this case, since only one integration is required, it is simpler to proceed by direct integration of the moment and then solve for M_Q. Assuming each segment is linearly elastic, has negligible shear deformation and undergoes small deflections, we can apply [21]:

$$\alpha(z_i) = \frac{dv}{dz_i} = \frac{1}{EI_i}\int M_i(z_i)\ dz_i, \tag{5}$$

where E is the Young's modulus of the material, and I_i is the moment of inertia of the segment. Integrating, augmenting (2), and evaluating at z_i^f, we can propagate the internal forces and deflection angles of each segment forward according to:

$$\begin{bmatrix} N_i \\ V_i \\ M_i \\ \hline \alpha_i(z_i^f) \end{bmatrix} = {}^i P_{i-1}^{aug} \begin{bmatrix} N_{i-1} \\ V_{i-1} \\ M_{i-1} \\ \hline \alpha_i(z_{i-1}^f) \end{bmatrix} \tag{6}$$

where

$${}^i P_{i-1}^{aug} = \left[\begin{array}{cccc|c} \cos(\theta_i-\theta_{i-1}) & -\sin(\theta_i-\theta_{i-1}) & 0 & 0 & 0 \\ \sin(\theta_i-\theta_{i-1}) & \cos(\theta_i-\theta_{i-1}) & 0 & 0 & 0 \\ z_i^f \sin(\theta_i-\theta_{i-1}) & z_i^f \cos(\theta_i-\theta_{i-1}) & 1 & 0 & 0 \\ \hline \frac{{z_i^f}^2}{2EI}\sin(\theta_i-\theta_{i-1}) & \frac{{z_i^f}^2}{2EI}\cos(\theta_i-\theta_{i-1}) & \frac{z_i^f}{EI} & 1 & 0 \\ \hline 0 & 0 & 0 & 0 & 1 \end{array}\right] \tag{7}$$

The compatibility conditions state that:

$$\begin{bmatrix} N_N \\ V_N \\ M_N \\ \hline \alpha_N(z_N^f) \end{bmatrix} = \begin{bmatrix} N_Q \\ V_Q \\ M_Q \\ \hline 0 \end{bmatrix}. \tag{8}$$

The first three equations are trivial, but the final equation can be solved to find the expression for the unknown internal moment M_Q in terms of F_{in} and F_{out}. Once this expression is determined, we can substitute it into the expression for M_R and propagate it outward using (2). We then proceed to find the expressions for the input displacement (displacement at Q along the direction of F_{in}), and the output displacement (displacement at R along the direction of F_{out}) using Castigliano's theorem.

Because the integration limits in this application of Castigliano's theorem are finite constants, and for a linearly elastic structure, the strain energy/per unit length will be continuous, we are permitted to bring the derivative inside the integral. Castigliano's theorem can then be expressed as:

$$\delta_j = \sum_{i=1}^{N}\int_0^{z_i^f} \left(\frac{M_i}{EI_i}\frac{\partial M_i}{\partial F_j} + \frac{2(\nu+1)V_i}{EA_i}\frac{\partial V_i}{\partial F_j} + \frac{N_i}{EA_i}\frac{\partial N_i}{\partial F_j}\right) dz_i, \tag{9}$$

where ν is the Poisson's ratio of the material, and A_i is the cross-sectional area of the segment. Since each of the internal forces and moments is linear in the loads F_j, we can use (2) to propagate the partial derivatives forward segment by segment, with the internal forces and moment replaced by their partial derivatives. Assuming each summand is calculated iteratively, $[\ N_{i-1}\ V_{i-1}\ M_{i-1}\ ]$ and their partial derivatives will not depend on z_i, and they can be pulled out of the integral. We can then express the output displacement as:

$$\delta_j = \sum_{i=1}^{N} \begin{bmatrix} N_{i-1} \\ V_{i-1} \\ M_{i-1} \end{bmatrix}^T Q_i \begin{bmatrix} \frac{\partial N_{i-1}}{\partial F_j} \\ \frac{\partial V_{i-1}}{\partial F_j} \\ \frac{\partial M_{i-1}}{\partial F_j} \end{bmatrix}, \tag{10}$$

where Q_i is as expressed as

$$Q_i = \int_0^{z_i^f} {}^i P_{i-1}^T \begin{bmatrix} \frac{1}{EA_i} & 0 & 0 \\ 0 & \frac{2(\nu+1)}{EA_i} & 0 \\ 0 & 0 & \frac{1}{EI_i} \end{bmatrix} {}^i P_{i-1}\ dz_i. \tag{11}$$

Performing the integration with respect to z_i, and assuming each segment has a rectangular cross section of width t_i, we obtain

$$\begin{aligned} Q_i &= \frac{1}{24EI_i}\begin{bmatrix} q_{11} & q_{12} & q_{13} \\ q_{21} & q_{22} & q_{23} \\ q_{31} & q_{32} & q_{33} \end{bmatrix} \\ q_{11} &= 2(z_i^f t_i^2 \cos^2(\theta_{i+1}-\theta_i) \\ &+ ((2\nu+1)z_i^f t_i^2 + 4{z_i^f}^3)\sin^2(\theta_{i+1}-\theta_i)) \\ q_{12}=q_{21} &= ((2\nu+1)z_i^f t_i^2 + 4{z_i^f}^3)\sin(2(\theta_{i+1}-\theta_i)) \\ q_{13}=q_{31} &= 12{z_i^f}^2\sin(\theta_{i+1}-\theta_i) \\ q_{22} &= 2(z_i^f t_i^2 \sin^2(\theta_{i+1}-\theta_i) \\ &+ ((2\nu+1)z_i^f t_i^2 + 4{z_i^f}^3)\cos^2(\theta_{i+1}-\theta_i)) \\ q_{23}=q_{32} &= 12{z_i^f}^2\cos(\theta_{i+1}-\theta_i) \\ q_{33} &= 24 z_i^f \end{aligned} \tag{12}$$

Before we can apply (10), we must perform a change of variable: $F = F_{in}/2$. This is necessary because the quarter actuator carries the 1/2 the input force, and taking the partial derivative with respect to the full input force F_{in} will yield

an erroneous result. To find the input displacement δ_{in}, we apply (10) with $F_j = F$. We then multiply this quantity by 2, since each half of the actuator undergoes this displacement. Applying (10) with $F_j = N_Q$ yields the displacement of point Q. Because of symmetry about B–B, we can simply multiply this by 2 to get the displacement of point P, or δ_{out}.

Because we have modeled each segment as a linearly elastic, Euler-Bernoulli beam with point loads, one would anticipate that the displacement expression will be linear in the loads multiplied by a multivariate cubic polynomial in d, h, and w. This is indeed the case. However, the application of the symmetric compatibility conditions along section A–A and B–B in Fig. 4 make the expression more complicated. We solved (6) for the unknown moment reaction M_Q, and this shows up in the denominator of the expression. Because the denominator of the displacement expression arises from the coefficient of the M_Q term in (6), the denominator will be first order in d, h, and w. However, looking at the *relative order* of the displacement expression (order of the numerator - order of the denominator), it is 3, the same order as a simple beam. If the structure is not rectangular, there are also trigonometric factors as part of these expressions. For this reason, it is advisable to keep the number of geometric parameters to a minimum, since the complexity of the expression will scale with the number of geometric parameters.

If we collect terms in the expressions for δ_{in} and δ_{out} with respect to the loads F_{in} and F_{out}, the denominator D_M will be common, up to a multiplicative constant. Therefore, we can write these equations as:

$$\begin{bmatrix} \delta_{in} \\ \delta_{out} \end{bmatrix} = \frac{1}{D_M} \begin{bmatrix} C_{11} & C_{12} \\ C_{21} & C_{22} \end{bmatrix} \begin{bmatrix} F_{in} \\ F_{out} \end{bmatrix}, \qquad (13)$$

where C_{ij} are quartic factors of the geometric parameters. The compliance matrix in this equation is precisely an immittance matrix of a two-port network. (Choosing displacement to be analogous to voltage makes it an admittance matrix). Its inverse is precisely the stiffness (impedance) matrix introduced in [15]. According to Maxwell's reciprocity theorem [4], at DC, the compliant mechanism will be a reciprocal two-port network. Therefore, following the notation in [15] we can write:

$$\begin{bmatrix} F_{in} \\ F_{out} \end{bmatrix} = \begin{bmatrix} s_1 & s_3 \\ s_3 & s_2 \end{bmatrix} \begin{bmatrix} \delta_{in} \\ \delta_{out} \end{bmatrix}, \qquad (14)$$

where s_1 corresponds to the stiffness in the input direction when the output is blocked, s_2 corresponds to the stiffness in the output direction when the previous amplification layer is completely rigid, and s_3 describes the cross-coupling from input to output, e.g. how much force is generated at a fixed output due to a given input displacement. s_3 also has units of stiffness. This matrix is positive definite; The combined effect of the stiffnesses in the input and output load's own direction will always be greater than the cross-coupling effect, due to the storage of strain energy in the compliance of the mechanism.

V. Model Validation by Finite Element Methods

The procedure in the previous section results in an analytical two-port model for a wide class of geometries. In order to implement this method, the designer must choose a reasonable set of geometric parameters that will be varied. The immittance matrix will be a function of these parameters. To demonstrate how this procedure works, we choose an octagonal mechanism ($N = 3$) of constant thickness ($t_i = t \quad \forall\ i$), varied its parameters and compared the analytical model's predictions to those produced using Finite Element Methods (FEM). The associated geometric parameters and the expected deformed shape with tensile input and output loads are shown in Fig. 5. Since the purpose of the FEM evaluation is merely to quantify how well the linear model performs compared to a numerical approach, $w/2 = 1$ m and $b = 2$ mm were chosen as general characteristic dimensions. This "meterstick" size gives an intuitive feel for how much deformation should occur, providing a useful check. As long as the size permits the device to be analyzed as a continuum, the mesh size will scale with the geometry of a given part, and for any characteristic dimension, the level of accuracy should be the same. In the actual application, w will be set by the previous layer and b is the thickness of the plate from which the compliant mechanism is machined, so we do not have absolute design authority over those parameters. The FEM evaluation varied d, θ, and t one at a time with the sum $h + 2d$ held equal to w. θ was held at $45°$ when it was not being varied, d was held at 500 mm when not being varied and t was held at 2 mm when not being varied. Loads were chosen for each geometry such that the mechanism would have a small, but visually discernible displacement at true scale.

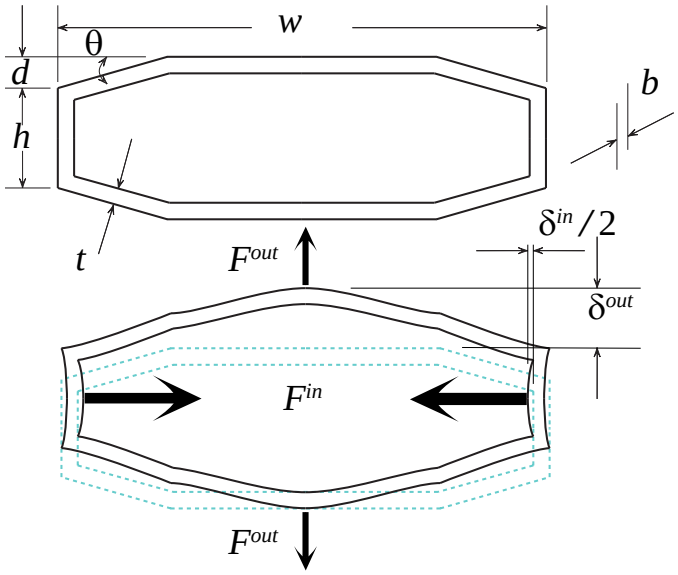

Fig. 5. Example parameters for model verification

We solved for the expressions in (13) using Wolfram Mathematica and evaluated them numerically for the various choices of geometric parameters. The expressions for D_M and the various C_{ij} can be found in Appendix B. We also simulated half the compliant mechanism for each set of parameters using Dassault Systèmes' SolidWorks Simulation finite element modeling software. The results for various geometries are shown in Tables I - VI. In the case of variation of the

Parameter	Value	Units
d	2.4	mm
h	1	mm
θ	6	°
t	0.15	mm

Fig. 6. Mechanism characteristics used in experiment. Parameters are as in Fig. 5

parameter t, the load was varied so as to keep the final displacement in a reasonable range. The level of agreement between the two methods is good, within 1% in most cases for thin mechanisms. As the ratio between t and w approaches 0.1, the accuracy begins to suffer, but for most useful compliant mechanisms, the ratio will be below this value.

VI. Experimental Results

In order to evaluate how well the expressions developed in the previous sections match the behavior of a true mechanism, we performed a series of experiments to measure the immittance parameters s_1, s_2, and s_3 for a representative strain amplifying structure. The mechanism we used was the outermost layer of an actuator for a biologically inspired camera positioner with 3 nested layers of amplification [23]. The full three-layer actuator has a predicted stroke length of 8.1 mm, with a resting length in the output direction of 20.6 mm. By way of comparison, 16 Cédrat APA50XS strain amplified PZT stacks placed in series would have a stroke length of 1.26 mm and a resting length in the output direction of 76.3 mm. The three-layer actuator uses 16 of these in its construction. The geometry of the compliant mechanism is of the class described in section V; it is a constant thickness mechanism whose geometry is parametrized by d, w, h, θ, and t. A photograph of the mechanism and the numerical values of its parameters are shown in Fig. 6. A rigid section was added to the middle to increase the height, because the chosen value of h does not allow enough space for the internal layers to be placed within this mechanism. The mechanism was machined from a 5mm thick plate of C655 High Silicon Bronze, which has an elastic modulus of 105 GPa and a Poisson's ratio of 0.346.

To identify s_1, s_2, and s_3 experimentally, we conducted two experiments. The first experiment (shown in Fig. 7) varied the output displacement with the input fixed and measured input and output force. The second experiment (shown in Fig. 8) varied the input displacement with the output free and measured input force and output displacement. Displacement (when it was the independent variable) was varied using a pair of NAI Aperture micropositioning stages. Force was measured using Futek LSB200 load cells and displacement (when it was the dependent variable) was measured using microepsilon OptoNCDT laser position sensors. s_1, s_2, and s_3 for this mechanism were determined from the combined data from both experiments using an unweighted least squares regression. Since the data was taken with either the input or output in a fixed or free condition, owing to the nature of the sensors, two experiments were necessary so that the measurements matrix would be full column rank. For instance, placing a load cell at the output would block the laser beam,

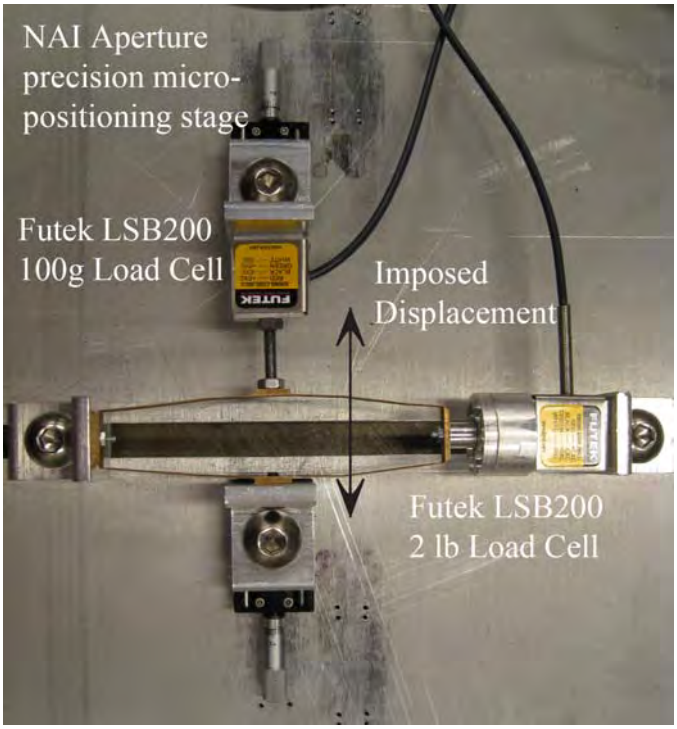

Fig. 7. First experiment (input fixed)

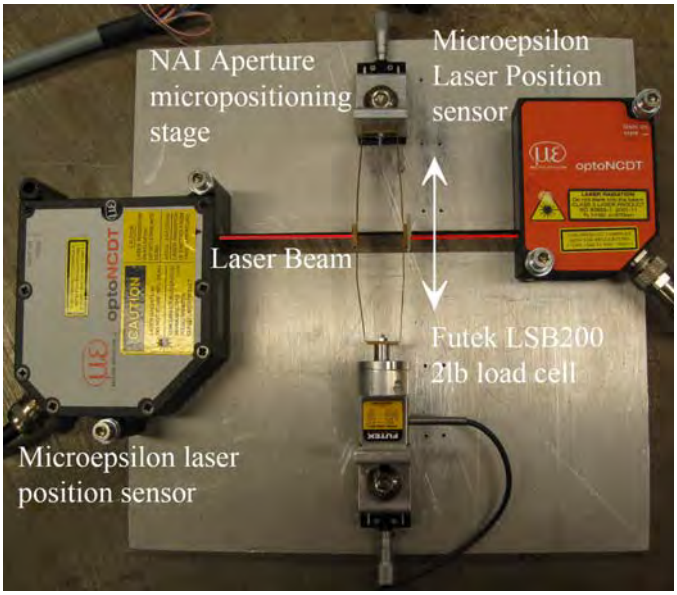

Fig. 8. Second experiment (output free)

so that output displacement and output force could not both be measured in the same experiment. Testing in a fixed or free condition gave us implicit knowledge that either a force or displacement was zero.

The results of the experiments are shown in Table VII. The analytical model predicts all parameters to within 18%.

VII. Discussion

The purpose of this theoretical construction of the various immittance parameters is not an end in itself. The goal of the

TABLE I
MECHANISM DISPLACEMENTS, VARYING d , h, F_{in} = 0.002 N, F_{out} = 0 N

d [mm]	δ_{in}			δ_{out}		
	FEM	Proposed Method	% difference	FEM	Proposed Method	% difference
2	1.481	1.488	0.47	-1.780	-1.787	0.39
5	1.486	1.487	0.06	-1.782	-1.788	0.34
10	1.479	1.485	0.41	-1.785	-1.791	0.34
50	1.469	1.473	0.27	-1.809	-1.816	0.39
200	1.404	1.409	0.35	-1.928	-1.816	6.16
500	1.225	1.230	0.41	-2.140	-2.127	0.61
900	0.932	0.937	0.54	-1.863	-1.870	0.37
990	0.847	0.852	0.59	-1.696	-1.700	0.23

TABLE II
MECHANISM DISPLACEMENTS, VARYING θ, F_{in} = 0.002 N, F_{out} = 0 N

θ [°]	δ_{in}			δ_{out}		
	FEM	Proposed Method	% difference	FEM	Proposed Method	% difference
85	1.462	1.468	0.49	-1.830	-1.836	0.33
80	1.442	1.448	0.42	-1.880	-1.884	0.21
70	1.398	1.404	0.43	-1.966	-1.971	0.26
60	1.344	1.350	0.44	-2.043	-2.048	0.26
30	0.967	0.971	0.41	-2.011	-2.018	0.36

TABLE III
MECHANISM DISPLACEMENTS, VARYING t, F_{in} VARIABLE, F_{out} = 0 N

d [mm]	F_{in} [N]	δ_{in}			δ_{out}		
		FEM	Proposed Method	% difference	FEM	Proposed Method	% difference
2	0.02	1.481	1.488	0.47	-1.780	-1.787	0.39
5	0.2	7.814	7.874	0.76	-13.50	-13.61	0.81
6		4.515	4.557	0.93	-7.804	-7.88	0.97
10	1	4.372	4.922	1.53	-8.377	-8.51	1.59
25	12	3.641	3.782	3.89	-6.285	-6.535	3.98
50	60	2.196	2.370	7.90	-3.779	-4.087	8.15
100	1200	5.131	5.978	16.5	-8.740	10.24	17.2

TABLE IV
MECHANISM DISPLACEMENTS, VARYING d , h, F_{in} = 0 N, F_{out} = 0.002 N

d [mm]	δ_{in}			δ_{out}		
	FEM	Proposed Method	% difference	FEM	Proposed Method	% difference
150	-9.43	-9.46	0.33	28.57	28.66	0.31
250	-9.84	-9.88	0.37	27.56	27.65	0.32
500	-10.57	-10.63	0.33	24.52	24.60	0.35
900	-9.31	-9.35	0.45	18.66	18.74	0.47
990	-8.40	-8.52	1.45	16.96	17.04	0.49

TABLE V
MECHANISM DISPLACEMENTS, VARYING θ, F_{in} = 0 N, F_{out} = 0.002 N

θ [°]	δ_{in}			δ_{out}		
	FEM	Proposed Method	% difference	FEM	Proposed Method	% difference
45	-10.57	-10.63	0.33	24.52	24.60	0.35
35	-10.47	-10.51	0.36	24.69	24.78	0.35
30	-10.05	-10.09	0.41	25.09	25.18	0.36
27.5	-9.56	-9.69	1.4	25.48	25.5	0.08

TABLE VI
MECHANISM DISPLACEMENTS, VARYING t, F_{in} = 0 N , F_{out} VARIABLE

d [mm]	F_{in} [N]	δ_{in}			δ_{out}		
		FEM	Proposed Method	% difference	FEM	Proposed Method	% difference
2	0.02	-10.57	-10.63	0.33	24.52	24.60	0.35
5	0.02	-0.6753	-0.6806	0.78	1.563	1.575	0.77
	0.2	-6.725	-6.806	1.2	15.45	15.75	1.94
10	2	-8.376	-8.508	1.58	19.39	19.68	1.50
25	24	-6.285	-6.535	3.98	14.56	15.13	3.91
50	60	-3.780	-4.087	8.12	8.778	9.472	7.91
100	1200	-8.748	-10.24	17.06	20.53	23.86	16.2

TABLE VII
MEASURED AND MODELED IMMITTANCES

Parameter	Analytical Model [N/m]	Experiment [N/m]
s_1	83400	80000
s_2	561	660
s_3	6560	5770

two-port model is to give a designer a simple model that can be used to make an informed choice of geometry in the first iteration of a design of the complete actuator, which consists of several compliant layers. The formulation of this model makes the traditional mechanics of materials assumptions of linearity and small deformations. In fact, the errors on each of the immittance parameters (which have units of stiffness) are on the order of errors found in experimental evaluations of flexure hinge stiffness [24]–[26]. Our evaluation is more complicated because we are trying to determine a matrix of values that correspond to coupled actions in orthogonal directions, not simply a stiffness in a given direction. Since the mechanism we evaluated was the outermost stage of a multistage amplification mechanism for robot-scale displacement, rather than a single-stage mechanism, as in previous works, the displacements are larger. One of the strengths of our modeling approach is that it allows for distributed compliance as well as localized compliance. We took advantage of this in the mechanism shown in Fig. 6. However, the drawback of distributed compliance is that the deformation can vary more widely with manufacturing tolerances. So it is understandable that our errors are slightly larger.

In addition, the mechanism considered represents an aggressive force-displacement tradeoff, and as a result, the surrounding region of the design space is very sensitive to parameter variations. This is illustrated in Fig. 9. When θ is small, varying θ while fixing d can be problematic because it can result in degenerate geometries, so to preserve valid geometries, $d = d' \tan\theta / \tan\theta'$ was chosen for the surface shown, where d' and θ' are the nominal values. Although a small change in one of the geometric parameters may affect blocked force and free displacement only slightly, the immittances can vary widely.

Because the mechanism we tested was so fragile, some permanent deformation occurred either through the manufacturing process or shipping and handling. We assumed that the immittances would not be largely changed by this deformation, but the residual stresses may have contributed to some of the error. There was some compliance inherent in the micropositioning stages and the load cells and this may have introduced some error in measurement. There also may have been some variation in the material constants from typical tabulated values.

VIII. USING ANALYTICAL TWO-PORT MODELS TO STUDY NESTED MECHANISMS

Although the full process of designing a multi-layer nested actuator is beyond the scope of this paper, we present the following discussion to show the usefulness of the the results in the earlier sections of this paper. We know that nested

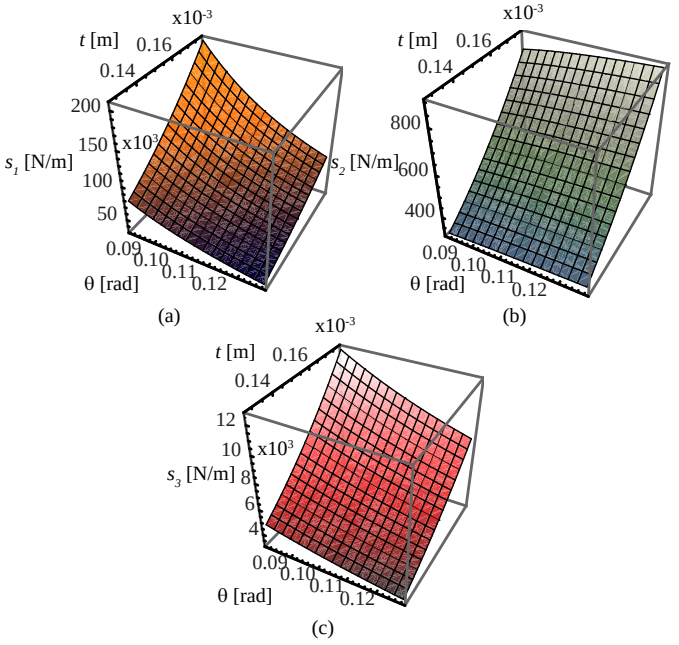

Fig. 9. Variation in immittance parameters: (a) s_1, (b) s_2, (c) s_3 with geometry

(a) two dimensional mechanism (b) three dimensional mechanism

Fig. 10. Multi-layer nested geometry with reuse of a compliant mechanism

mechanisms can produce more aggressive force-displacement tradeoffs than a single compliant mechanism, thus reaching larger stroke lengths without drastically increasing the resting length of the actuator. We also know that each time we add a layer, some strain energy is stored in the compliant mechanism, so unlike the idealized mechanism, we can not say the the amplification effect is simply multiplicative. The two-port network formalism allows us to analyze the effect of adding successive layers of strain amplification, determine if adding an additional layer is really a good idea, and estimate the point of diminishing returns.

Suppose that someone has designed a rhomboidal compliant mechanism to amplify the displacement a piezoelectric stack that satisfies manufacturing constraints. This "two-dimensional" mechanism is shown in Fig. 10a. However, let us also suppose that this mechanism has a blocked force in excess of the requirements and does not meet the stroke length requirements. How much does the designer gain by reusing the same compliant mechanism to amplify the displacement still further, generating the "three dimensional" mechanism shown in Fig. 10b?

A. Analysis of 3D nested structure with two identical compliant mechanisms

Let us suppose that the expressions for the immittance matrix have been determined for the compliant mechanism used in Fig 10a. The two-port force-displacement relationship can then be expressed as in (14), where s_1, s_2, and s_3 have units of stiffness, and each are expressions of the geometric parameterization and material properties.

In order to represent the cascaded connection of two strain amplification mechanisms, we need to use a different immittance matrix, the forward transmission matrix. This relationship expresses a different input-output choice for the same two-port model. Fortunately, the forward transmission matrix can be calculated directly following the procedure in [18] and is expressed as follows:

$$\begin{bmatrix} -\delta_{out} \\ F_{out} \end{bmatrix} = \frac{1}{s_3} \begin{bmatrix} s_1 & -1 \\ -\Delta & s_2 \end{bmatrix} \begin{bmatrix} \delta_{in} \\ F_{in} \end{bmatrix}, \qquad (15)$$

where Δ represents the determinant of the stiffness matrix in (14). δ_{out} is negated to represent the change of direction of displacement with each added layer in the hierarchy. It is more advantageous to tabulate and experimentally test the stiffness matrix in (14) than the forward transfer matrix because the stiffness matrix has consistent units among all the elements, whereas the forward transfer matrix does not.

The forward transfer characteristic of the cascaded connection of two nested compliant mechanisms is simply the product of the two forward transfer matrices. Denoting the stiffness matrix elements for each layer with a leading superscript, beginning with the innermost, we obtain the combined forward transfer characteristic:

$$\begin{bmatrix} \delta_{out} \\ F_{out} \end{bmatrix} = \frac{1}{{}^1s_3^2 s_3} * \begin{bmatrix} {}^1s_1\ {}^2s_1 + {}^1\Delta & -{}^1s_2\ -{}^2\ s_1 \\ -{}^2\Delta\ {}^1s_1 - {}^1\ \Delta\ {}^2s_2 & {}^2\Delta + {}^1\ s_2\ {}^2s_2 \end{bmatrix} \begin{bmatrix} \delta_{in} \\ F_{in} \end{bmatrix}, \qquad (16)$$

the negative sign having canceled out due to the direction being reversed twice. If the two mechanisms are the same, as in Fig 10b, the leading superscripts are unnecessary, and (16) becomes

$$\begin{bmatrix} \delta_{out} \\ F_{out} \end{bmatrix} = \frac{1}{s_3^2} \begin{bmatrix} s_1^2 + \Delta & -s_1 - s_2 \\ -\Delta(s_1 + s_2) & \Delta + s_2^2 \end{bmatrix} \begin{bmatrix} \delta_{in} \\ F_{in} \end{bmatrix}. \qquad (17)$$

B. Displacement amplification figure of merit

One important metric for strain amplified piezoelectric stacks is their *free displacement*, or the displacement of the output when no load is applied. This is synonymous with the maximum stroke length. One good dimensionless figure of merit that will tell us whether we should add another instance of a given mechanism to amplify the displacement still further is the ratio of the free displacements of the three dimensional mechanism in Fig. 10b to the two dimensional mechanism in Fig 10a. From (14) and (17) it can be shown that

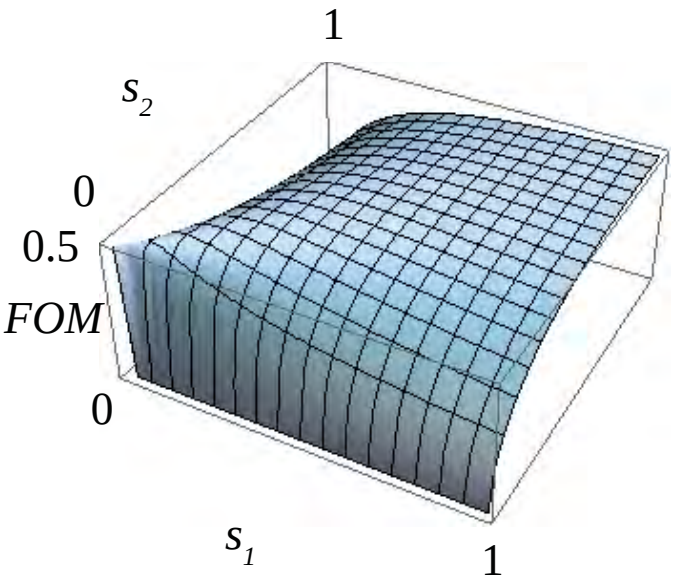

Fig. 11. Bounding surface on figure of merit over s_1,s_2

$$FOM = \frac{\mid \delta_{3D}^{free} \mid}{\mid \delta_{2D}^{free} \mid} = \frac{s_3}{s_1 + s_2} \qquad (18)$$

If this figure of merit is greater than one, it is worth adding another instance of the compliant mechanism to amplify the displacement still further. However, since the stiffness matrix must be positive definite, this figure is upper bounded by $\frac{\sqrt{s_1 s_2}}{s_1 + s_2}$. Therefore, the figure of merit must lie below the surface shown in Fig. 11. Because we have the analytical expressions for the two-port model of the mechanism, we can look at the figure of merit as it varies with *geometric* parameters. As an example, variation with thickness and angle are plotted in Fig. 12 over a wide range of values. The maximum value is around 0.5. This suggests that there is nothing to be gained by adding another instance of a known compliant mechanism; the free displacement is actually lower!

This is not to suggest a figure of merit greater than one cannot be achieved when the two layers are allowed to vary independently, in fact, previous work [15], [17], [27] indicates that this is possible. In each of these cases, the geometry of the outer layer is drastically different from the inner layer. The process for optimizing multi-layer mechanisms is quite involved and will not be discussed here. This involves further results on nested mechanisms that are the subject of a future work. The availability of analytical expressions for the two-port immittance parameters allows us to quickly evaluate nested topologies and determine whether there is a good range of geometric parameters for a given performance characteristic, something that is not easily done with purely numerical models, such as finite element methods.

IX. Conclusion

Piezoelectric stack actuators have the potential to be of great usefulness in robotics applications, but are limited by their low strain rate. This can be mitigated by the use of compliant strain

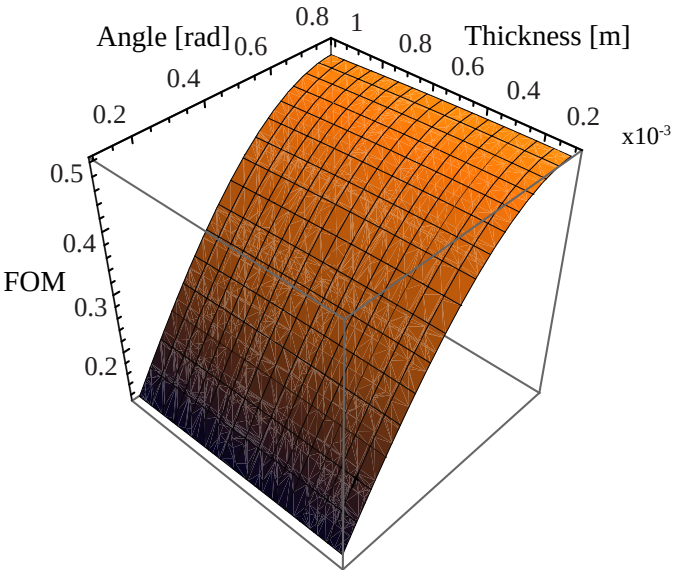

Fig. 12. Variation of figure of merit with angle and thickness

amplification mechanisms. This research presents a generalized Euler-Bernoulli formulation for the two-port model of any doubly symmetric strain amplification mechanism composed of a single loop of initially straight rectilinear segments. Unlike previous works, which either present purely numerical two-port models, or lists of long expressions, we provide analytical two-port expressions. This higher level of abstraction is a prerequisite for studying interconnections of these units because without it the expressions can become unwieldy, as well as topologically troublesome. A motivating example is shown for a particular class of mechanism described by 5 geometric parameters. The model for this example has been verified by finite element models. In addition, a particular mechanism of this type has been evaluated experimentally and shows good agreement, with an accuracy better than 18%. The analytical model for the two-port network can be used to eliminate guesswork as to how many layers of amplification should be used in a nested compliant mechanism. In future work, we will discuss further interesting properties that emerge in nested compliant mechanisms and show how the models developed in this article are used to choose geometries of each layer in response to desired performance specifications.

Appendix A
Two Port Network Models

Fig. 13 illustrates a two-port network with variable voltage and current at each port. Of the four input-output quantities of interest, V_1, V_2, I_1, I_2, any two, (e.g. both currents) can be designated as inputs, making the other two quantities (e.g. both voltages) outputs. The input-output relationship is then described by a 2×2 *immittance* matrix. If the four elements of the immittance matrix are known for a single choice of inputs, the immittance matrices for all remaining input-output relationships can be expressed as functions of the elements of this first immittance matrix.

For example, if the currents, I_1 and I_2 are chosen as inputs, then the voltages, V_1 and V_2, are outputs, then the immittance

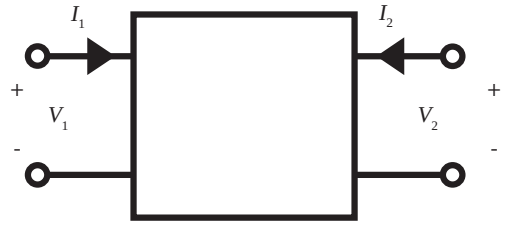

Fig. 13. Two-port electrical network model

matrix elements are impedances, and the relationship is as follows:

$$\begin{bmatrix} V_1 \\ V_2 \end{bmatrix} = \begin{bmatrix} Z_{11} & Z_{12} \\ Z_{21} & Z_{22} \end{bmatrix} \begin{bmatrix} I_1 \\ I_2 \end{bmatrix} \tag{19}$$

If $Z_{21} = Z_{12}$, then the network is termed a *reciprocal* two-port network [18], [28]. If $Z_{21} \neq 0$ and $Z_{12} \neq 0$, the network is termed a *bilateral* two-port, that is, changes in port 2 affect port 1, and vice versa [28]. Various relationships for interconnections of two-port networks have derived, which can be found in [18], greatly facilitating the analysis of complicated interconnected networks. For this reason, two-port networks have found great utility in the field of telemanipulation [28], [29].

Appendix B
Analytical Expressions for an Octagonal Mechanism with a Single Thickness

The various C_{ij} derived by solving the force-displacement relations using Castigliano's theorem are as follows:

$$\begin{aligned} C_{11} = &-\csc^2\left(\frac{\theta}{2}\right)\sec^4\left(\frac{\theta}{2}\right)\left(96d^4\cos(\theta) - 64d^4\cos(2\theta)\right. \\ &+ 32d^4\cos(3\theta) - 64d^4 - 64d^3h\sin(\theta) \\ &- 64d^3h\sin(3\theta) - 64d^3w\sin(\theta) - 64d^3w\sin(3\theta) \\ &+ 64d^2t^2\cos(2\theta) - 54.144d^2t^2\cos(3\theta) \\ &+ 11.072d^2t^2\cos(4\theta) + 16d^2\cos(\theta)\left(3.384t^2 + 3w^2\right) \\ &- 75.072d^2t^2 - 48d^2w^2\cos(3\theta) - 86dht^2\sin(\theta) \\ &+ 11.072dht^2\sin(2\theta) + 34dht^2\sin(3\theta) - 5.536dht^2\sin(4\theta) \\ &- 6dht^2\sin(5\theta) + 2dht^2\sin(7\theta) - 129.216dt^2w\sin(\theta) \\ &+ 11.072dt^2w\sin(2\theta) + 43.072dt^2w\sin(3\theta) \\ &- 5.536dt^2w\sin(4\theta) - 48dw^3\sin(\theta) + 16dw^3\sin(3\theta) \\ &- 5h^2t^2\cos(\theta) + 14h^2t^2\cos(2\theta) + 5h^2t^2\cos(3\theta) \\ &- 4h^2t^2\cos(4\theta) - h^2t^2\cos(5\theta) + 2h^2t^2\cos(6\theta) \\ &+ h^2t^2\cos(7\theta) - 12h^2t^2 - hw\cos(\theta)\left(18.536t^2 + 8w^2\right) \\ &+ 2hw\cos(2\theta)\left(20.536t^2 + 8w^2\right) + 18.536ht^2w\cos(3\theta) \\ &- 4ht^2w\cos(4\theta) - ht^2w\cos(5\theta) + 2ht^2w\cos(6\theta) \\ &+ ht^2w\cos(7\theta) - 39.072ht^2w + 8hw^3\cos(3\theta) - 16hw^3 \\ &- 2w^2\cos(\theta)\left(6.768t^2 + w^2\right) + 4w^2\cos(2\theta)\left(6.768t^2 + w^2\right) \\ &\left.+13.536t^2w^2\cos(3\theta) - 27.072t^2w^2 + 2w^4\cos(3\theta) - 4w^4\right) \end{aligned} \tag{20}$$

$$
\begin{aligned}
C_{21} = C_{12} = 2\big(&128d^4\csc^3(\theta) - 128d^4\csc(\theta) \\
&+ 384d^4\cot^2(\theta)\csc(\theta) - 512d^4\cot(\theta)\csc^2(\theta) \\
&+ 384d^3h\cot^2(\theta) + 1152d^3h\csc^2(\theta) \\
&- 512d^3(2h-w)\cot(\theta)\csc(\theta) - 1152d^3h - 12d^2h^2\cos^2(\theta) \\
&- 24d^2h^2\cos(\theta) + 9d^2h^2\cos(2\theta) \\
&+ 120d^2h^2\cot^2(\theta) + 258d^2h^2\csc^2(\theta) + 6d^2h^2\cos^2(\theta)\cot^2(\theta) \\
&- 24d^2h^2\cos(\theta)\cot^2(\theta) - 360d^2h^2\cot(\theta)\csc(\theta) \\
&- 249d^2h^2 - 541.44d^2t^2\sin(\theta) - 866.304d^2t^2\cot(\theta) \\
&+ 324.864d^2t^2\cos(\theta)\cot(\theta) + 64d^2\csc(\theta)\left(8.46t^2 - 6w^2\right) \\
&+ 64dht^2\cos^4(\theta) - 128dht^2\cos^3(\theta) + 128dht^2\cos^2(\theta) \\
&+ 32dht^2\cos(2\theta) + 56dht^2\cos(4\theta) + 384dht^2\sin^2(\theta)\cos(\theta) \\
&- 128dt^2(4.384h + 3.384w)\cos(\theta) - 24dht^2 - 384dhw^2 \\
&- 96h^2w^2 - 128ht^2(h+w)\sin(\theta)\cos^3(\theta) \\
&+ 128ht^2(h+w)\sin^3(\theta)\cos(\theta)\big)
\end{aligned} \tag{21}
$$

$$
\begin{aligned}
C_{22} = 2\big(&512d^4\csc^2(\theta) - 2048d^4\cot(\theta)\csc(\theta) \\
&- 3072d^3h\cot(\theta) + 1024d^3(h+w)\csc(\theta) + \\
&192d^2h^2\sin(\theta) - 1440d^2h^2\cot(\theta) + 576d^2h^2\csc(\theta) \\
&+ 192d^2h^2\cos(\theta)\cot(\theta) + 1536d^2hw - 386.304d^2t^2\cos(\theta) \\
&+ 256d^2t^2\cot^2(\theta) + 768d^2t^2\csc^2(\theta) \\
&- 32d^2t^2\cos(\theta)\cot^2(\theta) - 992d^2t^2\cot(\theta)\csc(\theta) \\
&+ 98.304d^2t^2 + 85dh^3\sin(\theta) + dh^3\sin(3\theta) \\
&- 2d\cot(\theta)\left(115h^3 + 322.58ht^2 + 256t^2w\right) \\
&+ 4d\csc(\theta)\left(43h^3 + 120.756ht^2 + 112t^2w\right) \\
&+ 16d\cos(\theta)\cot(\theta)\left(5h^3 + 12.46ht^2 + 4t^2w\right) \\
&- dh\left(h^2 + 1.692t^2\right)\cos^4(\theta)\cot(\theta) \\
&+ 2dh\left(h^2 - 126.308t^2\right)\sin(\theta)\cos^3(\theta) \\
&+ 4dh\left(h^2 + 1.692t^2\right)\cos^3(\theta)\cot(\theta) \\
&- dh\cos^2(\theta)\cot(\theta)\left(96dh + 25\left(h^2 + 1.692t^2\right)\right) \\
&+ dh\left(3h^2 + 261.076t^2\right)\sin^3(\theta)\cos(\theta) \\
&- dh\sin(\theta)\cos(\theta)\left(96dh + 29h^2 + 305.068t^2\right) \\
&+ 768dh^2w + 416.972dht^2\sin(\theta) + 33.692dht^2\sin(3\theta) \\
&+ 384dht^2\sin(\theta)\cos^2(\theta) + 241.152dt^2w\sin(\theta) \\
&+ 32h^4 + 128h^3w + 16h^2t^2\cos(2\theta) - 28h^2t^2\cos(4\theta) \\
&+ 260.576h^2t^2 - 32ht^2(h+w)\cos^4(\theta) + 16ht^2w\cos(2\theta) \\
&- 28ht^2w\cos(4\theta) + 388.576ht^2w + 128t^2w^2\big)
\end{aligned} \tag{22}
$$

the denominator common to all terms is:

$$
D_M = 6144\ E\ I\ \ (h + w - 2d(\cot\theta - \csc\theta)). \tag{23}
$$

To obtain the immittances in stiffness matrix form, we take:

$$
s_1 = \frac{C_{11}D_M}{C_{11}C_{22} - C_{21}^2} \tag{24}
$$

$$
s_2 = \frac{C_{22}D_M}{C_{11}C_{22} - C_{21}^2} \tag{25}
$$

$$
s_3 = \frac{-C_{21}D_M}{C_{11}C_{22} - C_{21}^2} \tag{26}
$$

ACKNOWLEDGMENT

This research was supported by NSF grant: Cyber-Physical Systems ECCS-0932208. Dr. Schultz was partially supported by a scholarship from the Achievement Rewards for College Scientists (ARCS) foundation when this research was conducted.

REFERENCES

[1] N. Hogan, *Multiple Muscle Systems*, J. Winters, Ed. Springer-Verlag, 1990.

[2] M. Frecker, "Recent advances in optimization of smart structures and actuators," *Journal of Intelligent Material Systems and Structures*, vol. 14, pp. 207–216, April-May 2003.

[3] S. Kota, K.-J. Lu, Z. Kreiner, B. Trease, J. Arenas, and J. Geiger, "Design and application of compliant mechanisms for surgical tools," *ASME Journal of Biomedical Engineering*, vol. 127, pp. 981–989, November 2005.

[4] M. Abdalla, M. Frecker, Z. Grdal, T. Johnson, and D. K. Lindner, "Design of a piezoelectric actuator and compliant mechansim combination for maximum energy efficiency," *Institute of Physics Smart Materials and Structures*, vol. 14, pp. 1421–1430, November 2005.

[5] S.-C. Huang and W.-L. Chen, "Design of topologically optimal microgripper," in *IEEE International Conference on Systems, Man and Cybernetics*, 2008.

[6] M. Grossard, C. Rotinat-Libersa, N. Chaillet, and M. Boukallel, "Mechanical and control-oriented design of a monolithic piezoelectric microgripper using a new topological optimization method," *Mechatronics, IEEE/ASME Transactions on*, vol. 14, no. 1, pp. 32 –45, feb. 2009.

[7] J. Paros and L. Weisbord, "How to design flexure hinges," *Machine Design*, vol. 37, no. 27, pp. 151–156, November 1965.

[8] N. Lobontiu, J. S. N. Paine, E. Garcia, and M. Goldfarb, "Corner-filleted flexure hinges," *Journal of Mechanical Design*, vol. 123, no. 3, pp. 346–352, 2001. [Online]. Available: http://link.aip.org/link/?JMD/123/346/1

[9] N. Lobontiu and E. Garcia, "Analytical model of displacement amplification and stiffness optimization for a class of flexure-based compliant mechanisms," *Computers & Structures*, vol. 81, no. 32, pp. 2797–2810, 2003.

[10] P. Mottard and Y. St-Amant, "Analysis of flexural hinge orientation for amplified piezo-driven actuators," *Smart Materials and Structures*, vol. 18, 3 2009.

[11] Y. Tian, B. Shirinzadeh, D. Zhang, and Y. Zhong, "Three flexure hinges for compliant mechanism designs based on dimensionless graph analysis," *Precision Engineering*, vol. 34, pp. 92–100, 2010.

[12] ——, "Closed-form compliance equations of filleted v-shaped flexure hinges for compliant mechanism design," *Precision Engineering*, vol. 34, pp. 408–418, 2010.

[13] R. Newnham, A. Dogan, Q. Xu, K. Onitsuka, J. Tressler, and S. Yoshikawa, "Flextensional "moonie" actuators," in *Ultrasonics Symposium*. IEEE, 1993, pp. 509–513.

[14] N. J. Conway, Z. J. Traina, and S.-G. Kim, "A strain amplifying piezoelectric mems actuator," *Institute of Physics Journal of Micromechanics and Microengineering*, vol. 17, pp. 781–787, 2007.

[15] J. Ueda, T. Secord, and H. Asada., "Large effective-strain piezoelectric actuators using nested cellular architecture with exponential strain amplification mechanisms," *IEEE/ASME Transactions on Mechatronics*, vol. 15, pp. 770–782, 2010.

[16] T. W. Secord and H. H. Asada, "A variable stiffness actuator with tunable resonance for cyclic motion tasks," in *IEEE International Conference on Robotics and Automation*, Kobe, Japan, May 2009, p. 176181.

[17] T. Secord and H. Asada, "A variable stiffness pzt actuator having tunable resonant frequencies," *Robotics, IEEE Transactions on*, vol. 26, no. 6, pp. 993 –1005, dec. 2010.

[18] J. Choma, Jr., *Electrical Networks: Theory and Analysis*. New York: John Wiley and Sons, Inc., 1985.

[19] J. Schultz and J. Ueda, "Analysis of antagonist stiffness for nested compliant mechanisms in agonist-antagonist arrangements," in *Proceedings of the ASME Dynamic Systems and Controls Conference*. Arlington, VA: ASME Dynamic Systems and Control Division, November 2011.

[20] S. Bharti and M. Frecker, "Compliant mechanical amplifier design using multiple optimally placed actuators," *Journal of Intelligent Material Systems and Structures*, vol. 18, pp. 209–217, March 2007.

[21] R. C. Juvinall and K. M. Marshek, *Fundamentals of Machine Component Design*, 3rd ed., J. Hayton, Ed. John Wiley and Sons, 2000.

[22] L. B. Y. U. Howell, *Compliant Mechanisms*, 1st ed. New York: John Wiley and Sons, 2001.

[23] J. Schultz, Joshua A; Ueda, "A Camera Positioner Driven by Muscle-Like Actuation," in *Proceedings of the IEEE International Conference on Biomedical Robotics & Biomechatronics (BioRob)*, Roma, Italy, 2012.

[24] N. Lobontiu and J. S. N. Paine, "Design of circular cross-section corner-filleted flexure hinges for three-dimensional compliant mechanisms," *ASME Journal of Mechanical Design*, vol. 124, pp. 479–484, September 2002.

[25] H.-H. Pham and I.-M. Chen, "Stiffness modeling of flexure parallel mechanism," *Precision Engineering*, vol. 29, pp. 467–478, 2005.

[26] G. Ye, W. Li, Y. qiao Wang, X. feng Yang, and L. Yu, "Kinematics analysis of bridge-type micro-displacement mechanism based on flexure hinge," in *Proceedings of the 2010 IEEE international conference on information and automation*, June 2010, pp. 66–70.

[27] E. E. Steltz, "Redesign of the micromechanical flying insect in a power density context," Ph.D. dissertation, University of California, Berkeley, May 2008.

[28] G. Raju, G. Verghese, and T. Sheridan, "Design issues in 2-port network models of bilateral remote manipulation," in *Robotics and Automation, 1989. Proceedings., 1989 IEEE International Conference on*, May 1989, pp. 1316 –1321 vol.3.

[29] M. Zareinejad, S. Rezaei, A. Abdullah, and S. S. Ghidary, "Development of a piezo-actuated micro-teleoperation system for cell manipulation," *The International Journal of Medical Robotics and Computer Assisted Surgery*, vol. 5, pp. 66–76, January 2009.